

# Time-dependent mean-field theory for x-ray near-edge spectroscopy

G. F. Bertsch<sup>1</sup> and A. J. Lee<sup>2</sup><sup>1</sup>*Institute for Nuclear Theory and Department of Physics, University of Washington, Seattle, Washington, USA*<sup>2</sup>*Department of Physics, University of Washington, Seattle, Washington, USA*

(Received 27 June 2013; revised manuscript received 31 January 2014; published 27 February 2014)

We derive equations of motion for calculating the near-edge x-ray absorption spectrum in molecules and condensed matter, based on a two-determinant approximation and Dirac's variational principle. The theory provides an exact solution for the linear response when the Hamiltonian or energy functional has only diagonal interactions in some basis. We numerically solve the equations to compare with the Mahan–Nozières–De Dominicis theory of the edge singularity in metallic conductors. Our extracted power-law exponents are similar to those of the analytic theory, but are not in quantitative agreement. The calculational method can be readily generalized to treat Kohn-Sham Hamiltonians with electron-electron interactions derived from correlation-exchange potentials.

DOI: [10.1103/PhysRevB.89.075135](https://doi.org/10.1103/PhysRevB.89.075135)

PACS number(s): 71.15.Mb, 78.70.Dm, 78.20.Bh

## I. INTRODUCTION

Time-dependent density functional theory (TDDFT) has proven to be a very useful tool for calculating the linear response of molecules and condensed matter systems. The overall features of the dielectric function are reproduced quite well, and the agreement at zero frequency in insulators is often at the few percent level. It also describes the plasmon peaks in the UV absorption spectrum and the corresponding energy loss spectrum in inelastic electron scattering.

The good experience in TDDFT in the optical regime encourages its application to x-ray absorption, which has a rich near-edge structure that is only partially described by single-electron physics. Indeed, some aspects of the x-ray response are accessible to TDDFT [1–4]. However, other aspects, particularly the dynamics of core-hole relaxation, are beyond the scope of the theory. This is because the fundamental assumption that the wave function be represented by a single Slater determinant is too restrictive when the core orbital is part of that determinant. In the single-determinant approximation for the linear response, most of the wave function is in the ground state. It requires at least two determinants to treat the effects of the core-hole potential. To overcome this deficiency, we propose here a theory based on two separate Slater determinants, one for the initial and another for the final state. We derive the equations of motion in Sec. II below. We refer the reader to Ref. [5] for an review of the foundations of TDDFT and its recent extensions. In Sec. III following we apply our extension to the well-known Mahan–Nozières–De Dominicis (MND) Hamiltonian. A comprehensive discussion of analytic and numerical methods to solve it is given in the review by Ohtaka and Tanabe [6]. The equations we solve numerically are exact for the MND Hamiltonian. We will argue that they are much easier than other methods to apply to DFT functionals which contain electron-electron interactions.

We note that a multicomponent TDDFT has already been derived as a generalization of the Runge-Gross theorem [10,11]. It can be motivated as follows [12]. The ansatz permits a closer approximation to the physical starting wave function, and thus the accompanying density functional is then likely to be amenable to a simpler approximation. However, the extensions derived from the Runge-Gross theorem are

typically based on a representation by particle-hole excitations of a single determinant [9]. Our derivation and equations of motion are different, resembling more the multideterminant theory of nuclear excitations proposed in Ref. [13]. There is no underlying functional in our treatment here, although the equations are motivated by TDDFT. Each Slater determinant has its own density and evolves with the Kohn-Sham equation based on that density.

The final time-dependent equation that we solve numerically is Eq. (15) below; the response is evaluated using Eqs. (13) and (16).

## II. THE TWO-DETERMINANT APPROXIMATION

We derive equations of motion from Dirac's variational principle

$$\delta \int dt \langle \Psi(t) | i \frac{d}{dt} - H | \Psi(t) \rangle = 0, \quad (1)$$

varying the wave function  $|\Psi\rangle$  in the space of Slater determinants. The resulting time-dependent Kohn-Sham (KS) equations are then solved for the time-dependent wave function  $|\Psi(t)\rangle$ . For discussion of the action principle in the context of TDDFT, see Refs. [7,8].

The linear response to an operator  $\mathcal{O}$  is obtained from the time-dependent correlator  $\langle [\mathcal{O}(t), \mathcal{O}(0)] \rangle / i$  calculated from

$$R(t) = \lim_{\lambda \rightarrow 0} \frac{1}{\lambda} \langle \Psi_\lambda(t) | \mathcal{O} | \Psi_\lambda(t) \rangle. \quad (2)$$

Here the initial state has been prepared by applying an impulsive field  $V(r,t) = \lambda \mathcal{O} \delta(t)$  to the KS ground state  $|\Psi_g\rangle$ . In linear order, this modifies the initial wave function to

$$|\Psi_\lambda(0_+)\rangle = (1 - i\lambda \mathcal{O}) |\Psi_g\rangle. \quad (3)$$

The resulting wave function is evolved by KS equations to determine the matrix element in Eq. (2). The connection of Eq. (2) to the more familiar frequency-dependent response  $S(\omega)$  is given by

$$S(\omega) \equiv \sum_f \langle f | \mathcal{O} | 0 \rangle^2 \delta(E_f - \omega) = \frac{1}{\pi} \int_0^\infty dt R(t) \sin \omega t. \quad (4)$$

Since  $\lambda$  is small in Eq. (2), the evolved wave function is still largely in the ground state with only a small amplitude of excited states. This is fatal for calculating effects of the core hole excitation such as the relaxation of the valence wave function in the presence of the core hole. By considering separate determinants for the components of the wave function with and without the core electron excitation, the correlations associated with valence electrons can be treated as well as they are in the optical response. There is no danger of violating the Fermi statistics because the two components of the wave function are necessarily orthogonal.

Our starting point is the following ansatz for the variational wave function:

$$|\Psi\rangle = a_g c_c^\dagger |\Psi_{vg}\rangle + a_c |\Psi_c\rangle. \quad (5)$$

Here  $|\Psi_{vg}\rangle = \prod_{\alpha}^{N_e} c_{\alpha}^\dagger$  is the Slater determinant of the valence electrons in a state with the core electron in its ground state orbital, where  $N_e$  is the number of active electrons in addition to the core electron. Correspondingly,  $|\Psi_c\rangle = \prod_{\beta}^{N_e+1} c_{\beta}^\dagger$  is the Slater determinant for a state with the excited core electron in the valence band. The two sets of valence-band orbitals are expressed in terms of the valence-band basis states  $i$  as  $c_{\alpha}^\dagger = \sum a_{\alpha i} c_i^\dagger$  and  $c_{\beta}^\dagger = \sum a_{\beta i} c_i^\dagger$  where  $a_{\alpha i}$  and  $a_{\beta i}$  are time-dependent amplitudes. We may choose these expansion coefficients to satisfy the conditions  $\sum_i a_{\alpha i}^* a_{\alpha' i} = \delta_{\alpha\alpha'}$ , etc. The amplitudes of the two Slater determinants (SDs)  $a_g(t)$  and  $a_c(t)$  will determine the mixing of the two determinants. They satisfy the normalization condition  $|a_g|^2 + |a_c|^2 = 1$ .

The MND Hamiltonian has the form

$$\hat{H} = \hat{H}_v(c_i^\dagger, c_i) + \hat{H}_c(c_i^\dagger, c_i) c_c c_c^\dagger. \quad (6)$$

The first term is the valence Hamiltonian to be constructed from the corresponding Kohn-Sham density functional. The second term adds the excitation energy of the core hole as well as its field acting on the valence electrons.

The variation in Eq. (1) is to be carried out with respect to changes in the wave function  $|\Psi\rangle$  that preserve its character as a sum of two SDs. In the single-determinant theory, one takes the variational derivatives of  $|\Psi\rangle$  with respect to  $a_{\alpha,i}$  treating them as independent variables. This results in the usual time-dependent Kohn-Sham (KS) with the single-particle Hamiltonian given by

$$\hat{H}_{KS} = \sum_{i,j} \langle \Psi | \frac{\delta^2 \hat{H}_v}{\delta c_i^\dagger \delta c_j} | \Psi \rangle c_i^\dagger s_{ij} c_j, \quad (7)$$

where  $s_{ij} = \pm 1$  is a phase factor depending on the ordering of the operators in  $\hat{H}_v$ . However, as a consequence of the overcompleteness of the variables, the overall phase of the time-dependent KS wave function no longer has any physical meaning. For example, if the orbitals are eigenstates of the KS Hamiltonian, the overall phase is  $\exp(-i \sum_n^{N_e} \epsilon_n t)$ , where  $\epsilon_n$  are the KS eigenvalues. The correct phase is  $\exp(-i \langle \Psi | H | \Psi \rangle t)$ ; the two are only equal in the absence of electron-electron interactions. This phase plays no role in the single-determinant theory, but with two determinants it is crucial to have correct relative phases.

The proper procedure to apply Eq. (1) is to require that the wave function variations in

$$\langle \delta \Psi | i \frac{d}{dt} - \hat{H} | \Psi(t) \rangle = 0 \quad (8)$$

are independent of each other. An orthogonal (and thus independent) set of wave function variations may be defined by making use of Thouless's representation [14] of the SDs. The equations of motion are obtained by taking  $|\delta \Psi\rangle$  as the set of 1-particle 1-hole excitations of the instantaneous SD,

$$|\delta \Psi\rangle \in |\alpha_p \alpha_h\rangle \equiv c_{\alpha_p}^\dagger c_{\alpha_h} |\Psi(t)\rangle, \quad (9)$$

in accordance with Thouless's theorem. For a state of  $N_e$  particles in a basis of dimension  $N_b$ , there are  $N_e(N_b - N_e)$  particle-hole amplitudes to be determined compared to the  $N_e N_b$  amplitudes in the representation Eq. (5). However, the use of Eq. (9) requires calculating both particle and hole orbitals in an instantaneous basis, which is very costly in carrying out the time evolution. An easier way to avoid the phase introduced by the Kohn-Sham single-particle Hamiltonian is by projection. The action of  $\hat{H}_{KS}$  on the SD can be expressed in the instantaneous particle-hole basis as

$$\hat{H}_{KS} |\Psi\rangle = E_{KS} |\Psi\rangle + \sum_{\alpha_p, \alpha_h} v(\alpha_p, \alpha_h) |\alpha_p \alpha_h\rangle, \quad (10)$$

where  $E_{KS} = \langle \Psi | \hat{H}_{KS} | \Psi \rangle$ . The unwanted first term can be removed in any basis simply by updating the wave function using the projected KS Hamiltonian  $\hat{H}_{KS} - E_{KS}$ . Thus, the single-particle orbitals are calculated as usual, but the phase of the SD is corrected by  $\exp(+i \langle \hat{H}_{KS} \rangle \Delta t)$  at each time step. For our numerical example below, the problem does not arise because there is no electron-electron interaction in the valence space.

To summarize, we solve independently the time-dependent Kohn-Sham equations for  $|\Psi_g\rangle$  and  $|\Psi_c\rangle$ . The two determinants are coupled by the x-ray photon interaction,

$$\hat{H}_x = v_x (c_x^\dagger c_c + c_c^\dagger c_x), \quad c_x^\dagger = \sum_i f_i c_i^\dagger \quad (11)$$

with  $f$  a form factor. Varying with respect to  $a_g, a_c$  one obtains the  $2 \times 2$  matrix equation for these variables,

$$i \frac{d}{dt} \begin{pmatrix} a_c \\ a_g \end{pmatrix} = a_c \begin{pmatrix} \langle \Psi_c | \hat{H} - E_{KS,c} | \Psi_c \rangle & v_x \langle \Psi_c | \hat{H}_x c_c^\dagger | \Psi_{vg} \rangle \\ v_x \langle \Psi_{vg} | c_c \hat{H}_x | \Psi_c \rangle & \langle \Psi_{vg} | \hat{H} - E_{KS,g} | \Psi_{vg} \rangle \end{pmatrix} \times \begin{pmatrix} a_c \\ a_g \end{pmatrix}. \quad (12)$$

The hermiticity of  $\hat{H}_x$  ensures that the normalization condition remains satisfied during the course of the evolution. The off-diagonal matrix element in this equation is expressible as the  $N+1 \times N+1$  determinant

$$\langle \Psi_c | c_x^\dagger | \Psi_{vg} \rangle = \begin{vmatrix} \langle \beta_1 | \alpha_1 \rangle & \dots & \langle \beta_1 | x \rangle \\ \langle \beta_2 | \alpha_1 \rangle & \dots & \\ \dots & & \\ \langle \beta_{N+1} | \alpha_1 \rangle & \dots & \langle \beta_{N+1} | x \rangle \end{vmatrix}. \quad (13)$$

While this determinant is well known in the analytic theory of the near-edge response [6], it is absent from the usual time-dependent Kohn-Sham theory based on a single Slater determinant.

To evaluate the linear response to the field of the x-ray photon, we start with the ground state wave function at time zero, which we call  $|\Psi_g(0)\rangle$ . We now perturb the system by an impulsive x-ray field,  $\lambda\hat{H}_x\delta(t)$ . The immediate evolution introduces a small component of the core-excited state into the wave function,

$$|\Psi(0_+)\rangle = |\Psi_g(0)\rangle + i\lambda v_x |\Psi_c(0)\rangle, \quad (14)$$

where  $|\Psi_c(0)\rangle = c_x^\dagger |\Psi_{vg}(0)\rangle$ . Equation (14) has the required form as a sum of two determinants. Each is evolved in time with its own Kohn-Sham Hamiltonian. The evolution of  $|\Psi_{vg}\rangle$  is trivial since the ground is stationary. All the dynamics come from the evolution of  $|\Psi_c\rangle$  by the time-dependent HS equations,

$$i \frac{da_{\beta i}}{dt} = \sum_j (i|\hat{H}_{KS}|j\rangle a_{\beta j} \text{ for } 1 \leq \beta \leq N_e + 1. \quad (15)$$

Then the real-time response from Eq. (2) is

$$R(t) = 2v_x^2 \text{Re}\langle \Psi_c(t) | c_x^\dagger | \Psi_{vg}(t) \rangle. \quad (16)$$

This can be easily Fourier transformed by Eq. (4) to give the absorption spectrum.

Our procedure provides an exact solution for the linear response if  $\hat{H}_v$  and  $\hat{H}_c$  are strictly one-body operators. This is because the intrinsically two-body part of the Hamiltonian does not make two-particle excitations or entangle the two Slater determinants after the initialization.

### III. NUMERICAL CALCULATIONS

In this section we demonstrate the practicality of the method as applied to the MND Hamiltonian. The computer codes employed here are available at Ref. [15].

We write the two terms in the Hamiltonian as

$$\hat{H}_v = \frac{E_b}{N_b - 1} \sum_{i=1}^{N_b} (i - N_b/2) c_i^\dagger c_i \quad (17)$$

and

$$\hat{H}_c = \frac{v_c}{N_b} c_x^\dagger c_x, \quad c_x^\dagger = \sum_i c_i^\dagger. \quad (18)$$

Here  $E_b$  is the width of the band, and  $N_b$  is the number of orbitals in the band. We shall express energies in units of  $E_b$ , and time in units of  $\hbar/E_b$ . We start with a half-filled band, taking the number of valence electrons  $N_e$  to be  $N_e = N_b/2$ . We present calculations for the parameter sets listed in Table I.

As explained in the literature [6], the core-hole interaction strength  $v_c$  is not the most physically direct quantity determining the near-edge response. The effect of the Fermi-surface edge is more closely related to the shift of the single-particle orbital energies due to the core hole. Calling the shift  $\Delta\varepsilon$ , the relevant quantity is

$$\Delta\varepsilon \frac{dn}{d\varepsilon} = \frac{\delta}{\pi}, \quad (19)$$

TABLE I. Parameter sets for the Hamiltonian Eqs. (17) and (18).

case	$N_b$	$N_e$	$v_c$	$\delta/\pi$
A	256	128	-0.8	0.38
B	8	4	-0.8	0.39
C	512	256	-0.8	0.38
Z	256	128	0	0

where  $dn/d\varepsilon$  is the density of orbital states at the Fermi level. In the last equality, this is related to the scattering phase shift  $\delta$  at the Fermi surface. The values of  $\delta$  associated with the computed parameter sets are given in the last column of Table I.

The Green's function theory in Ref. [16] for the time-dependent response decomposes it into two factors, the overlap of Fermi sea determinants and the Green's function of the electron that was promoted to the valence band. We write the overlap of the Fermi sea determinants as

$$G(t) = \langle \Psi_{vg} | e^{-i(\hat{H}_v + \hat{H}_c)t} | \Psi_{vg} \rangle. \quad (20)$$

The main quantity of interest is the determinant in Eq. (16) which we call  $g_c$ , as

$$g_c(t) = \langle \Psi_c(t) | c_x^\dagger | \Psi_{vg}(0) \rangle. \quad (21)$$

Nozières and De Dominicis decompose it into two factors,  $g_c(t) = g(t)G(t)$ . We will not make use of that separation.

#### A. Fermi sea evolution

We first examine the Fermi sea overlap. To remove the phase of the core-excited ground state, we will examine the quantity

$$G'(t) = e^{i \sum_\alpha \varepsilon_\alpha t} \langle \Psi_{vg} | e^{-i(\hat{H}_v + \hat{H}_c)t} | \Psi_{vg} \rangle, \quad (22)$$

where  $\varepsilon_\alpha$  are the Kohn-Sham eigenvalues of the ground-state orbitals. Figure 1 shows  $\text{Re}G'(t)$  for parameter set A of Table I. It is plotted on a log-log scale to facilitate comparison with result of Ref. [16],

$$G(t) \sim (1/t)^{(\delta/\pi)^2}. \quad (23)$$

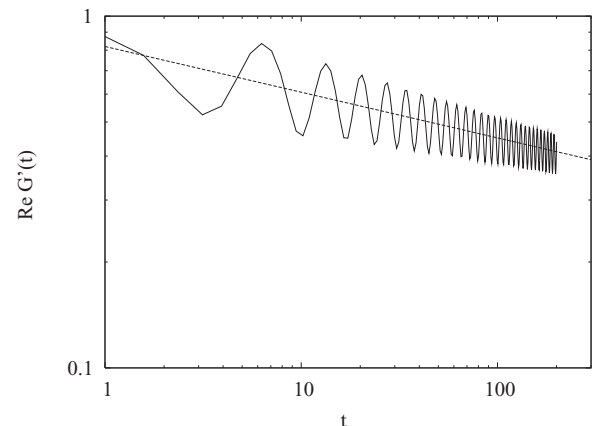


FIG. 1.  $\text{Re}G'(t)$  as a function of time for parameter set A. The line shows a visual power-law fit,  $G'(t) \sim t^{-0.13}$ .

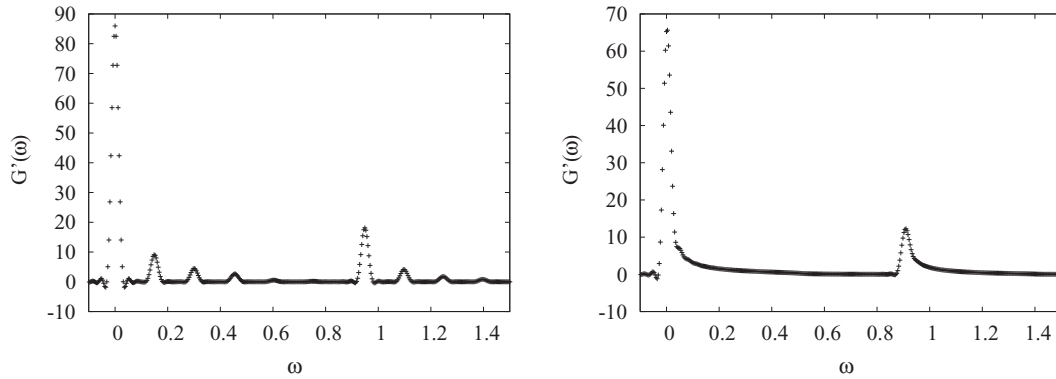


FIG. 2.  $\text{Re}G'(\omega)$  as a function of  $\omega$ . Left-hand panel: Results for a low-dimensional system, parameter set B. Right-hand panel: Results for parameter set A.

The predicted power-law dependence should be applicable over the time domain starting from  $t_0 \sim 1/E_b$  and going to  $t_1 \sim dn/d\varepsilon = N_b/E_b$ , the time necessary to resolve individual orbitals in the band. In our units the range is  $(t_0, t_1) = (1, N_b)$ . One notices immediately that  $G'(t)$  has a considerable oscillatory component. The oscillation has been found in other treatments of the problem as well, e.g., Eq. (3.4) of Ref. [17]. As discussed in Ref. [6], the oscillation may be attributed to the deeply bound orbital at the bottom edge of the valence band.

The line in the graph corresponds to the power law  $G(t) \sim (1/t)^\gamma$  with  $\gamma = 0.13$ . This is rather close to the predicted power law derived in Ref. [16],  $\gamma = (\delta/\pi)^2 \approx 0.14$ .

The spectral function associated with  $G'(t)$  is its Fourier transform,

$$G'(\omega) = \int_0^\infty dt e^{i\omega t} G'(t). \quad (24)$$

Figure 2 plots  $\text{Re}G'(\omega)$  for parameter sets A and B. For the set A shown in the left-hand panel one can see the peaks associated with individual states of the many-particle wave function. The dimension of the many-particle space is given by  $\binom{N_b}{N_c} = 20$ . The ground state is the peak on the far left, and 8–9 other states are visible in the plot. The right-hand plot shows  $\text{Re}G'(\omega)$  for parameter set A. Here the individual states are so closely spaced that one can see only smooth curves. There are clearly two peaks in the spectrum, one associated with the ground state and its low-energy excitations, and the other associated with a localized orbital bound or nearly bound to the core hole. The secondary peak was discussed in Ref. [18] and also recently in Ref. [19]. In Fig. 3 we have replotted the  $\text{Re}G'(\omega)$  ground-state peak on a log-log scale to make visible a power-law dependence on  $\omega$ . The expected range of validity for a power law is within the interval  $(\omega_0, \omega_1) = (1/N_b, 1)$  in our units. The line in Fig. 3 shows the power law  $\omega^{-1.13}$ . We can see that it provides a reasonable fit in the range (0.02, 0.3) with some oscillation at low frequency.

### B. Inclusion of the core electron

We now examine the propagation of the core-hole excited determinant with the core electron promoted to the valence band. The number of electrons in the determinant is now  $N_b/2 + 1$ . The initial wave function has equal amplitudes for

the  $x$  electron in all the unoccupied orbitals; it thus has the same localization as the core-hole potential. Just as a reminder of the noninteracting physics, we show in Fig. 4 the imaginary part of  $g_c(\omega)$  at  $v_c = 0$ . It is uniform across the region of unoccupied orbitals, with sharp edges at the Fermi surface and at the top of the band. The right-hand panel shows the Green's function with parameter set A. Note that the peak associated with a hole at the bottom of the valence band is missing. Evidently, the electron added by  $c_x^\dagger$  operator ensures with a high probability that the hole is filled. The results in the right-hand panel are plotted in Fig. 5 on a log-log scale. The line is a visual fit to power-law behavior. Evidently, a power law gives a reasonable description over the energy interval 0.02–0.3. According to the theory, the exponent is determined by the phase shift according to the dependence<sup>1</sup>

$$\gamma = -2\frac{\delta}{\pi} + \frac{\delta^2}{\pi^2}. \quad (25)$$

Taking  $\delta/\pi$  from Table I, the predicted value is  $\gamma = -0.62$ , compared to  $\gamma = -0.85$  from the fit.

The small disagreement we find here persists over a large range of  $\delta$ . Figure 6 shows a comparison over the range of  $\delta$  accessible to the Hamiltonian. We see that the exponent is

<sup>1</sup>This is for a single partial wave and spin projection.

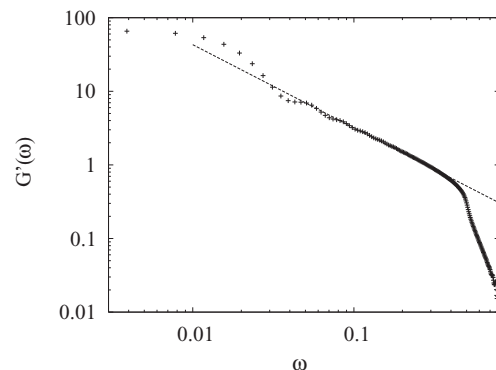


FIG. 3. The same  $G'(\omega)$  as in Fig. 2(b), plotted on a log-log scale. The line shows a visual power-law fit,  $G'(\omega) \sim \omega^{-1.13}$ .

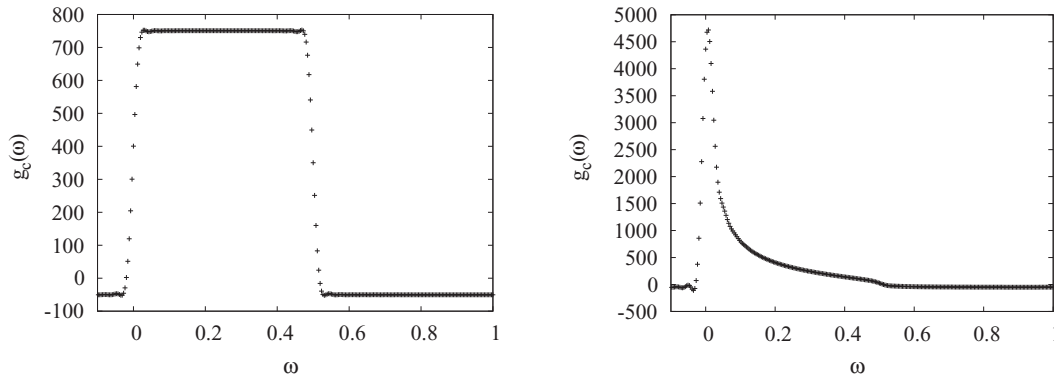


FIG. 4. Left panel: Core-excited Green's function with no interaction, parameter set Z. Right panel: The same quantity with parameter set A. Note the difference in vertical scale.

proportional to  $\delta$  for small  $\delta$  as in Eq. (25), but the coefficient is somewhat higher.

### C. Other numerical treatments

Various numerical treatments of the MND Hamiltonian have been discussed and reviewed in Ref. [6]. The two main approaches are the Green's function formulation [17,20–23] and the formulation in terms of many-body determinantal wave functions [24–28]. The former requires constructing functions of at least two variables in the time or frequency domain, governed by equations that are nonlocal in those variables. In this respect, the real-time wave function method is much more efficient since there is only one time variable and the equations to be solved are local in time. An early numerical work following the wave function approach is Ref. [24]. These authors constructed the numerically exact solutions of the core-hole excited Hamiltonian, and then used the ground state and one-particle excitations of the Hamiltonian as the final states. This procedure of enumerating the eigenstates was also used in Ref. [27]. The wave function approach was also used in Ref. [28], and the determinant was evaluated in real time, as in our approach. However, the procedure adopted there was based on the formulation of Ref. [18] which requires a

matrix inversion. The near singularity of the matrix apparently caused numerical difficulties that do not arise in the real-time approach. From a computational point of view, our approach is closest to that used in Refs. [25] and [26]. We note that these authors found that the critical exponents of the analytic Green's function treatment were only in qualitative agreement with the numerical results outside of a very small interval near  $\omega = 0$ .

### IV. SUMMARY AND OUTLOOK

We have derived an extension of time-dependent density functional theory that contains at least some of the subtle many-particle physics of x-ray near-edge absorption in metals. Numerically, the real-time theory is easy to carry out if the time-dependent electron-electron interaction is neglected. The absorption shows that the x-ray absorption power-law behavior is in qualitative agreement with the analytic results of Ref. [30], but not identical to them. A similar conclusion was obtained in Ref. [25].

Physically, the most important effect of the many-electron physics is core-hole screening. There are several numerical calculations in the literature that follow the Green's function formalism of Ref. [16] and focus on this screening effect. For

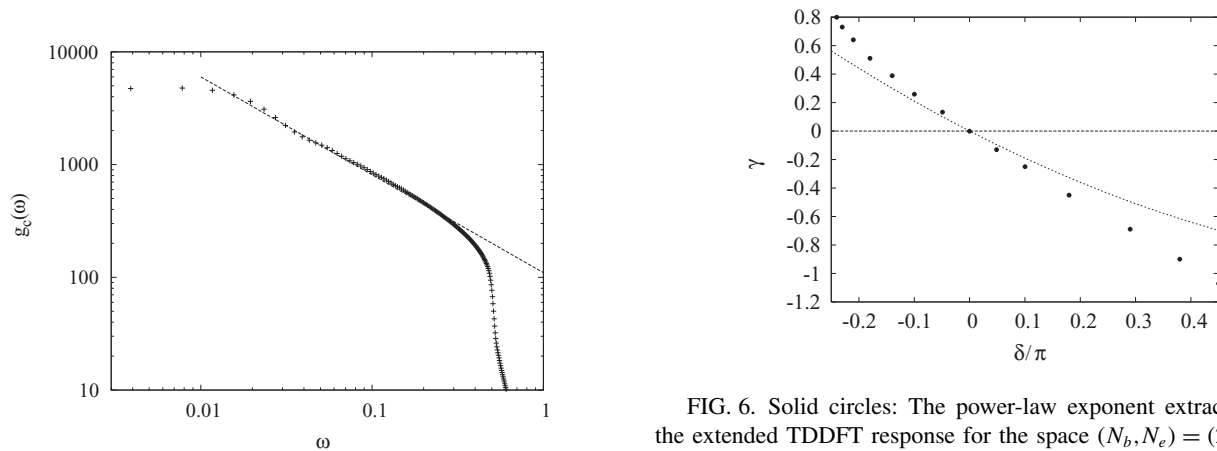


FIG. 5. The determinant  $g_c(\omega)$ , plotted on a log-log scale. The line shows an approximate power-law fit,  $g_c(\omega) \sim \omega^{-0.85}$ .

FIG. 6. Solid circles: The power-law exponent extracted from the extended TDDFT response for the space  $(N_b, N_e) = (256, 128)$ . Dashed line: The analytic formula Eq. (25). The numerically computed exponent was extracted from the calculated  $g_c(\omega)$  at  $\omega = 0.03$  and  $0.2$ .

the absorption spectra, a commonly used approximation treats the system as fully relaxed in the presence of the core hole. Good fits can also be obtained under the assumption that the dynamic screening reduces the core-hole effects by a factor of two [4]. That work also presented a real-time dynamic calculation, but apparently used a diagonal approximation to Eq. (16). In any case, dynamic effects related to the core hole can be easily calculated in the real-time method, so there is no reason to use any of these approximations.

So far we have not discussed the electron-electron interactions within the valence band. They are potentially important and are needed to treat the additional screening associated with the plasmon degree of freedom. Langreth has proposed a way to include plasmon effects in the Green's function approach [29] and it was applied with some success in Ref. [31]. However, it involves distinct calculations for the plasmon physics and for the x-ray absorption. In contrast, the real-time TDDFT provides a unified framework for including the electron-electron interaction in the calculation. In the

two-determinant theory one can simply add the Coulomb field of the instantaneous charge density of  $|\Psi_c\rangle$  to the field generated by  $v_c$ . Of course, the presence of the interaction requires considerably more computational effort. The Coulomb field has to be calculated at each time step. Also, the overall phase of the  $|\Psi_c\rangle$  has to be computed using one of the methods discussed in Sec. II. We believe that the problem is still computationally quite tractable; we leave the implementation to a future publication.

#### ACKNOWLEDGMENTS

We acknowledge discussions with J. J. Rehr, A. Bulgac, and K. Yabana and helpful comments from C. Ullrich. We also thank U. Mosel for bringing Ref. [19] to our attention. This work was supported by the National Science Foundation under Grant No. PHY-0835543 and by the US Department of Energy under Grant Nos. DE-FG03-97ER4563 and DE-FG02-00ER41132.

- 
- [1] M. P. Prange, J. J. Rehr, G. Rivas, J. J. Kas, and J. W. Lawson, *Phys. Rev. B* **80**, 155110 (2009).
  - [2] A. Sakko, A. Rubio, M. Hakala, and K. Hamalainen, *J. Chem. Phys.* **133**, 174111 (2010).
  - [3] K. Lopata, B. Van Kuiken, M. Khalil, and N. Govind, *J. Chem. Theory Comput.* **8**, 3284 (2012).
  - [4] A. J. Lee, F. D. Vila, and J. J. Rehr, *Phys. Rev. B* **86**, 115107 (2012).
  - [5] M. Marque, N. Maitra, F. Nogueira, and E. Gross (eds.), *Fundamentals of Time-Dependent Density-Functional Theory*, Lecture Notes in Physics, Vol. 837 (Springer, Berlin, 2012).
  - [6] K. Ohtaka and Y. Tanabe, *Rev. Mod. Phys.* **62**, 929 (1990).
  - [7] G. Vignale, *Phys. Rev. A* **77**, 062511 (2008).
  - [8] M. Ruggenthaler and R. van Leeuwen, in Ref. [5], pp. 206-210.
  - [9] R. van Leeuwen and E. Gross, in Ref. [5], p. 249.
  - [10] M. Beck, A. Jäckle, G. Worth, and H.-D. Meyer, *Phys. Rep.* **324**, 1 (2000).
  - [11] O. Alon, *J. Chem. Phys.* **127**, 154103 (2007).
  - [12] C. A. Ullrich, *Time-Dependent Density-Functional Theory: Concepts and Applications* (Oxford University Press, Oxford, 2011).
  - [13] G. Puddu, *Int. J. Mod. Phys. E* **22**, 1350040 (2013).
  - [14] P. Ring and P. Schuck, *The Nuclear Many-Body Problem* (Springer, Berlin, 1980).
  - [15] See Supplemental Material at <http://link.aps.org/supplemental/10.1103/PhysRevB.89.075135> for the computer codes used for the calculations.
  - [16] P. Nozières and C. T. De Dominicis, *Phys. Rev.* **178**, 1097 (1969).
  - [17] K. Ohtaka and Y. Tanabe, *Phys. Rev. B* **34**, 3717 (1986).
  - [18] M. Combescot and P. Nozières, *J. Phys. (Paris)* **32**, 913 (1971).
  - [19] M. Knap, A. Shashi, Y. Nishida, A. Imambekov, D. A. Abanin, and E. Demler, *Phys. Rev. X* **2**, 041020 (2012).
  - [20] K. Schönhammer and O. Gunnarsson, *Solid State Commun.* **23**, 691 (1977).
  - [21] V. Grebennikov, Y. Babanov, and O. Sokolov, *Phys. Status Solidi B* **80**, 73 (1977).
  - [22] T. Privalov, F. Gel'mukhanov, and H. Agren, *Phys. Rev. B* **64**, 165115 (2001).
  - [23] U. von Barth and G. Grossmann, *Phys. Scr.* **21**, 580 (1980).
  - [24] A. Kotani and Y. Toyozawa, *J. Phys. Soc. Jpn.* **35**, 1082 (1973).
  - [25] C. A. Swartz, J. D. Dow, and C. P. Flynn, *Phys. Rev. Lett.* **43**, 158 (1979).
  - [26] J. Dow and C. Flynn, *J. Phys. C* **13**, 1341 (1980).
  - [27] L. A. Feldkamp and L. C. Davis, *Phys. Rev. B* **22**, 4994 (1980).
  - [28] G. D. Mahan, *Phys. Rev. B* **21**, 1421 (1980).
  - [29] D. C. Langreth, *Phys. Rev. B* **1**, 471 (1970).
  - [30] B. Roulet, J. Gavoret, and P. Nozières, *Phys. Rev.* **178**, 1072 (1969).
  - [31] M. Guzzo, J. Kas, and F. Sottile, *Eur. Phys. J. B* **85**, 324 (2012).